Er^{3+} interlayer energy migration as the limiting photoluminescence quenching factor in nanostructured Er^{3+}:Y_2O_3 thin films

J. Hoang,[1] Robert N. Schwartz,[2] Kang L. Wang,[2] and J. P. Chang[1]
[1]*Department of Chemical and Biomolecular Engineering, University of California, Los Angeles, California 90095, USA*
[2]*Department of Electrical Engineering, University of California, Los Angeles, California 90095, USA*

(Received 13 November 2011; accepted 2 July 2012; published online 25 July 2012)

We report the effects of Er^{3+} nanostructuring on optical properties of heterogeneously doped Er^{3+}:Y_2O_3 thin films synthesized by radical enhanced atomic layer deposition. By alternating the cycle sequences of Y_2O_3 and Er_2O_3, rare earth (RE) ion concentrations were controlled from 4.8 to 11.8 at. % Er and the local Er_2O_3 thicknesses were varied between 0.7 to 7.6 Å. Photoluminescence (PL) was used to examine the 1535 nm (Er $^4I_{13/2}\rightarrow{}^4I_{15/2}$) emission at two excitation wavelengths, 488 nm and 976 nm. The normalized PL increased with increasing Er^{3+} concentrations up to 11.8 and 9.6 at. % under 488 and 976 nm excitations, respectively. The introduction of a local Er_2O_3 layer greater than 2.4 Å resulted in significant PL quenching, over an order of magnitude, under both excitation wavelengths. The quenching was attributed to enhanced local $Er^{3+}\leftrightarrow Er^{3+}$ interlayer energy migration. Compared to homogeneously doped RE systems where the RE concentration is directly related to the average RE↔RE spatial distance, increased luminescence was observed at high Er^{3+} concentrations in heterogeneously doped systems. These results suggest that controlling the RE proximity is key to engineering the optical properties of RE doped heterogeneous materials. © *2012 American Institute of Physics*. [http://dx.doi.org/10.1063/1.4737793]

I. INTRODUCTION

Optical materials have found use in a wide range of applications ranging from photovoltaics, solid state lighting, and fiber optics to sensors.[1–4] One element of particular interest is erbium. Due to the multiple energy level splitting characteristic of Er^{3+}, upconversion,[5] photoluminescence,[6] and downconversion[7] have been demonstrated in Er^{3+} doped material systems with the goal of optimizing emission yields for a particular wavelength of interest. Considerable work has focused on enhancing the 1535 nm emission corresponding to the Er $^4I_{13/2}\rightarrow{}^4I_{15/2}$ transition to create materials suitable for compact amplifier designs.[8] A major challenge in scaling down the Er^{3+} doped material systems is achieving a high fraction of optically active Er^{3+} ions while circumventing the quenching of Er $^4I_{13/2}\rightarrow{}^4I_{15/2}$ emission, which has been attributed to high Er concentration,[9,10] impurities,[2,11] cooperative upconversion,[12,13] and excited state absorption.[14,15] The majority of studies have focused on homogeneously distributed Er^{3+} ions, while few have focused on heterogeneously doped films despite reports of significantly higher active Er^{3+} concentrations before PL quenching is observed.[16–18] As a result, it is of interest to investigate the effect of the Er^{3+} distribution on the 1535 nm emission with emphasis on achieving high active Er^{3+} concentrations while minimizing quenching effects.

Figure 1 shows a comparison between homogeneous Er^{3+} doped films and heterogeneous nanolaminate films formed by a layer-by-layer deposition approach. For both film types, an increase in the Er^{3+} at. % effectively decreases the average $Er^{3+}\leftrightarrow Er^{3+}$ ion proximity. The main difference is that for homogeneously doped films the Er^{3+} concentration is directly coupled to the $Er^{3+}\leftrightarrow Er^{3+}$ proximity, whereas for the heterogeneously doped films the local Er^{3+} distribution can be altered. More specifically, control of nanostructuring (defined as the local Er_2O_3 thickness) and separation between the Er_2O_3 layers can be achieved through nanolaminates with alternating oxide structures (e.g. Er_2O_3 and Y_2O_3). The use of layer-by-layer deposition to study energy transfer is not new, but the sub-nanometer control achieved in this work is novel. Serna *et al.*[18] used pulsed laser deposition to deposit films consisting of Er^{3+} separated by 3 to 9 nm of Al_2O_3. They showed evidence of $Er^{3+}\leftrightarrow Er^{3+}$ interlayer excitation migration based on observed changes in the Er $^4I_{13/2}\rightarrow{}^4I_{15/2}$ lifetime and the 1.54 μm PL intensity. Unfortunately, Er clustering may have contributed to the observed changes, and the parameter space investigated was one where relatively weak excitation migration was expected to occur based on resonant energy theory. According to resonant energy theory, $Er^{3+}\leftrightarrow Er^{3+}$ dipole-dipole energy transfer follows a $1/R^6$ dependence, where R is the distance between the interacting ions.[19,20] This means that for shorter $Er^{3+}\leftrightarrow Er^{3+}$ proximities, excitation migration is strong. For this reason, it is of interest to study energy transfer for sub-nanometer $Er^{3+}\leftrightarrow Er^{3+}$ proximities, especially for cases in which the active Er^{3+} concentration is high, and luminescence quenching is weak.

We previously reported on Er_2O_3 nanostructuring in an Y_2O_3 host by radical enhanced atomic layer deposition (RE-ALD), where the 1535 nm Er emission was assessed as a function of Er^{3+} concentration using a 488 nm Ar laser.[17] Luminescence quenching was observed after more than 8 at. % Er was incorporated in Y_2O_3, which is a significantly larger active Er^{3+} concentration compared to ion implanted homogeneous Er^{3+} doped films that typically contain less than 1 at. % Er.[13,21] Based on X-ray absorption spectroscopy (XAS), it was determined that Er was six fold coordinated to

 © 2012 American Institute of Physics

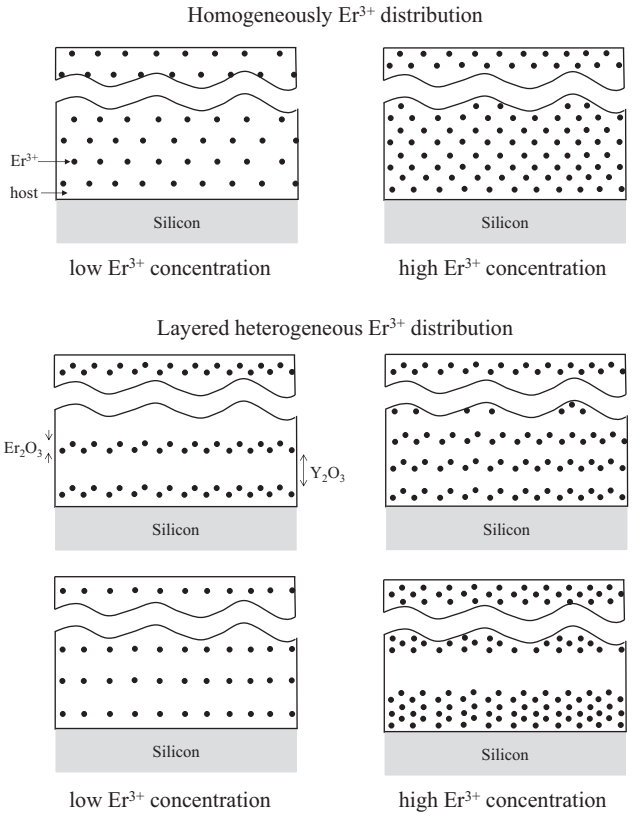

FIG. 1. Schematic of nanostructured films that were deposited using different local Y_2O_3:Er_2O_3 cycle sequences.

oxygen; therefore, no Er clustering was evident in the films leading to the conclusion that $Er^{3+}\leftrightarrow Er^{3+}$ ion interactions from nanostructured local Er_2O_3 layers led to PL quenching above 8 at. % Er. The layer-by-layer nature of RE-ALD facilitates the control of the Er concentration, proximity, and nanostructuring with films that are cluster-free. These attributes make it possible to assess spatial and concentration effects on PL.

In this work, nanostructured heterogeneous Er^{3+} doped Y_2O_3 of varying Er^{3+} concentrations, $Er_2O_3\leftrightarrow Er_2O_3$ proximity, and local Er_2O_3 thicknesses were synthesized using RE-ALD to assess their effects on the Er^{3+} 1535 nm luminescence under 488 nm and 976 nm excitations. We note that the parameters investigated were strongly interrelated (e.g. an increase in Er^{3+} concentration results in a change in $Er^{3+}\leftrightarrow Er^{3+}$ proximity), but the thin film heterogeneity resulting from layer by layer growth enabled a spatial study of Er^{3+} interactions in the film growth direction.

II. EXPERIMENTAL SETUP

A detailed description of the ultra-high vacuum chamber, process conditions, and experimental technique have been discussed previously, so only a brief description is included here.[16,22] Thin films of Er-doped Y_2O_3 were deposited on Si (100) substrates at 350 °C using RE-ALD. The precursors of choice were metal β-diketonates, $M(TMHD)_3$ (M = Y or Er), with oxygen atoms as the oxidant. Y_2O_3 and Er_2O_3 were deposited with a pulsing sequence of 10 s of precursor, 5 s of pumping-down, 30 s of atomic oxygen exposure, followed by another 5 s pump-down period. Nanostructuring and spatial control of Er^{3+} in Y_2O_3 samples was achieved by alternating the deposition cycles of Y_2O_3 and Er_2O_3. Previous work confirmed the nanostructuring using transmission electron microscopy and extended X-ray absorption fine structure analysis.[17] Subatomic growth of Y_2O_3 and Er_2O_3 was achieved for each cycle such that the average distance between Er_2O_3 layers and local Er_2O_3 thickness could be investigated in the subnanometer length scale. Switching oxides during ALD of nanolaminates has been reported to change the growth rate and has been attributed to changes in nucleation.[23] As the film thickness does not necessarily correlate to the number of ALD cycles in nanolaminates, a wide range of cycle sequences was used to investigate Er_2O_3 nanostructuring and proximity.

The spatial distribution was studied using an Y_2O_3:$Er_2O_3 = a$:1 local cycle sequence, where a is 0, 1, 5, 10, and 15. Nanostructuring was studied using 4 different Y_2O_3:Er_2O_3 local cycle sequences: (i) b:b with b equal to 1, 5, 10, and 15, (ii) 10:c with c equal to 1, 5, and 10, (iii) 15:d with d equal to 1, 5, 10, and 15, and (iv) f:5 with f equal to 5, 10, and 15. Er^{3+}:Y_2O_3 films of 70.5 to 136 nm were grown by repeating the local deposition sequence by at least 75 times. The film composition and erbium concentration, [Er], was determined with X-Ray photoelectron spectroscopy (XPS), using a monochromatic Al source on a Kratos Axis Ultra XPS system with take-off angles of 90° with respect to the sample surface. A survey spectrum using a pass energy of 80 eV yielding a step size of 0.5 eV was performed to determine the surface elements. The spectrum was referenced to the C-C 1 s binding energy at 285 eV.

The film thickness of Er^{3+}:Y_2O_3 was determined to be between 70.5 to 136 nm by spectroscopic ellipsometry (J. A. Woollam M-88) using an optical model of Y_2O_3. Assuming –CH and -OH impurities were homogeneously distributed in the film, the local RE oxide thickness was estimated by dividing the film thickness as measured by spectroscopic ellipsometry by the total number of deposition sequences used, then scaling this number with the measured RE concentrations.

Photoluminescence (PL) measurements were performed at room temperature on Er-doped Y_2O_3 films using an Ar laser (488 nm) and a laser diode (976 nm). The estimated spot size based on the focal length of the mirror and a beam diameter of 2 mm was 46 μm and 93 μm for the Ar source and laser diode source, respectively. Using the beam diameters, photon fluxes were estimated to be $8.9\times10^{22}\,cm^{-2}s^{-1}$ and $3.6\times10^{22}\,cm^{-2}s^{-1}$ for the Ar laser and laser diode sources, respectively. A liquid nitrogen cooled Princeton OMA V InGaAs detector was used to collect spectra from 900 to 1650 nm. To assess the effects of Er concentration, interlayer Er_2O_3 spacing, and Er_2O_3 nanostructuring, backgrounds were subtracted from the PL spectra, and the spectra were integrated from 1400 to 1620 nm. The integrated PL was then normalized to provide an accurate comparison.[24] The effects of the parameters under investigation were described in terms of two factors: a normalized PL and an effective Er PL yield. The normalized PL was defined as:

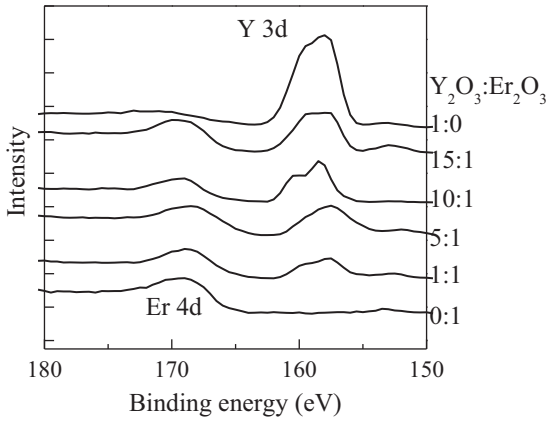

FIG. 2. XPS spectra of Er^{3+}:Y_2O_3 films synthesized with an Y_2O_3:$Er_2O_3 = a$:1 cycle sequence, showing Y 3d and Er 4 d,with reference to pure Er_2O_3 and Y_2O_3 thin films.

$$\overline{PL} = \frac{integrated\ PL\ intensity}{film\ thickness}. \quad (1)$$

This parameter was used for quantitative comparisons between thin film materials with different structural properties and RE doping concentrations.

The effective Er PL yield was determined by:

$$Y_{\overline{PL}} = \frac{\overline{PL}}{Er\ concentration} = \frac{\overline{PL}}{[Er]}. \quad (2)$$

This factor represents an effective efficiency for the conversion of the excitation photon wavelength (e.g. 488 or 976 nm) to the desired wavelength of 1535 nm for Er^{3+}. As these values were unique to the PL measurement setup, they were assessed in terms of relative changes in magnitudes.

III. RESULTS AND DISCUSSION

Figure 2 shows the XPS spectra for the *a*:1 cycle sequence in comparison to Y_2O_3 and Er_2O_3 thin films. The Y 3 d and Er 4 d peaks were clearly visible in the Er^{3+}:Y_2O_3 films and showed an increase in the Y 3 d intensity and corresponding decrease in Er 4 d intensity as the number of Y_2O_3 cycles *a* increased. Figure 3 shows the RE concentrations calculated based on the XPS measurements along with the corresponding RE oxide thicknesses from the *a*:1 deposition sequence. It shows that a change in Y_2O_3 cycles *a* from 1 to 15 resulted in an increase in Y concentration from 5.2 to 9.6 at. % with a corresponding decrease in Er concentration from 11.8 at. % to 4.8 at. %, affirming the RE concentration control by sequential deposition using ALD. The estimated local RE oxide film thicknesses showed that both the Y_2O_3 and Er_2O_3 thicknesses increased with increasing *a* cycles. The increase in Y_2O_3 thickness was expected, but that in Er_2O_3 thickness was not. This pseudo-ALD deposition condition may be a result of some $Er(TMHD)_3$ precursor decomposition at longer dwell time. Precursor decomposition could lead to the adsorption of larger and potentially non-volatile organic ligands thereby reducing the removal rate of organic groups by atomic oxygen. This deposition artifact could potentially be fixed by introducing a timed purge line on the precursor housing. For the purpose of this work, the obtained control of the local film thickness was sufficient to study local RE interaction effects. For the *a*:1 sequence, Y_2O_3 and Er_2O_3 thicknesses were from 0.3 to 3.7 Å and from 0.7 to 2.6 Å, respectively. These thicknesses were much smaller than the $Er^{3+} \leftrightarrow Er^{3+}$ nanostructure studies achieved using pulsed laser deposition by Serna *et al.*, which was able to achieve a spacing of 3 to 9 nm.[18] The other deposition sequences showed similar increases in thickness and concentration as the number of Y_2O_3 and Er_2O_3 cycles increased (not shown).

PL spectra of a 9.6 at. % Er^{3+} doped thin film under 488 nm and 976 nm excitations are shown in Figure 4. Under 488 nm excitation, the PL spectrum clearly showed the characteristic luminescence from the Er $^4I_{13/2} \rightarrow {}^4I_{15/2}$ transitions. The main peak occurred at 1535 nm and had a full width at half max (FWHM) of ~21 nm. In addition, there were a major shoulder centered at ~1546 nm and a broad minor one in the 1480 nm range. The PL spectrum under 976 nm excitation showed significantly more noise, consistent with the smaller absorption cross-section of Er $^4I_{11/2}$ compared to that of Er $^4F_{7/2}$. This noise could also be attributed to efficient energy transfer to the Si substrate. The PL spectra of all ALD films shared similar characteristic features.

The effect of interlayer Er_2O_3 spacing on PL was investigated using an Y_2O_3:$Er_2O_3 = a$:1 deposition sequence. The deposition sequence facilitated the investigation of PL as a

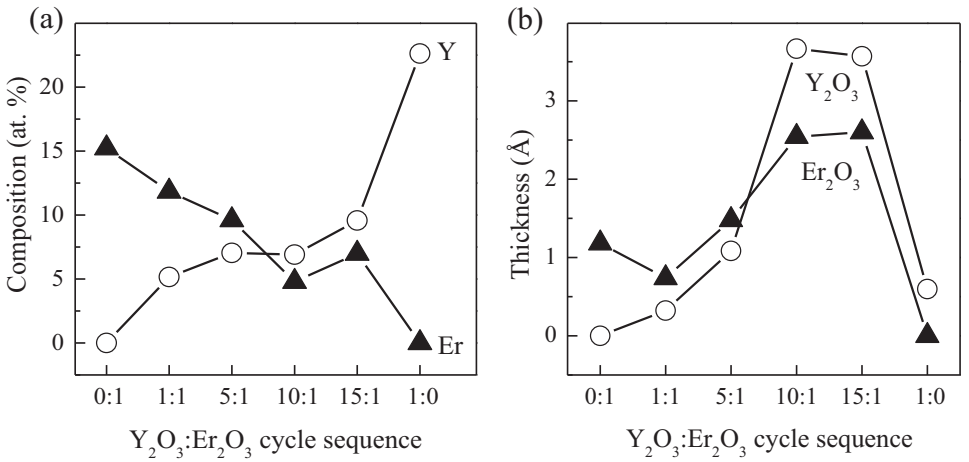

FIG. 3. (a) RE concentrations (b) average Y_2O_3 and Er_2O_3 thicknesses for Er^{3+}:Y_2O_3 films synthesized with an *a*:1 Y_2O_3:Er_2O_3 cycle sequence.

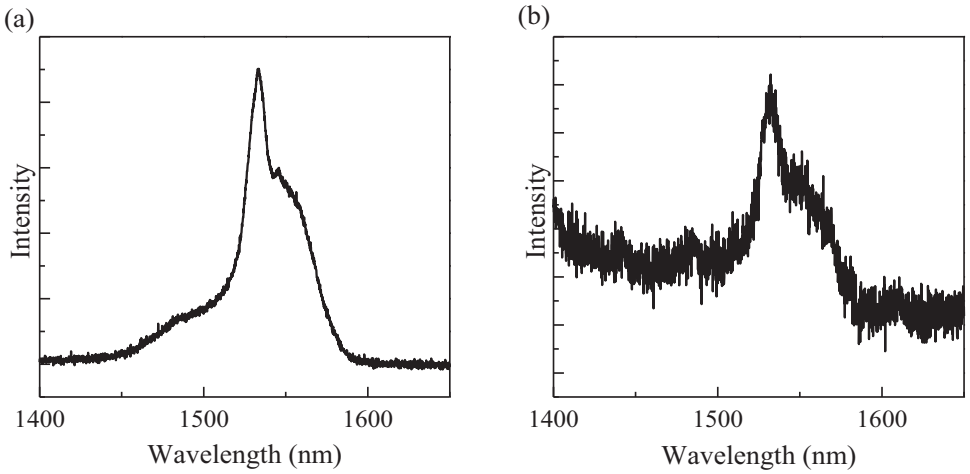

FIG. 4. Photoluminescence spectra for 9.6 at. % Er^{3+}:Y_2O_3 film (deposited with an Y_2O_3:Er_2O_3 = 5:1 cycle sequence) under (a) 488 nm and (b) 976 nm excitation wavelengths.

function of the Er_2O_3 separation, since the Y_2O_3 thickness increased with increasing *a*. As the Y_2O_3 thickness increased, the effective Er PL yield showed a general increase under both excitation wavelengths (not shown). As shown in Figure 5 under 488 nm excitation, the normalized PL increased with increasing Er concentration up to 11.8 at. % and thereafter quenched. This optimum Er concentration for peak normalized PL was higher than previously reported[17] and was partially attributed to lower carbon contamination levels leading to reduced migration to quenching impurities. The data point where quenching occurred corresponded to a pure Er_2O_3 thin film. Under 976 nm excitation, the normalized PL increased significantly with increasing Er concentration up to 7.0 at. % then increased steadily up to 9.6 at. % and was followed by luminescence quenching. The saturation-like behavior of the PL increase with Er concentration was indicative of higher order excitation processes such as cooperative upconversion and excited state absorption (ESA). All PL spectra under 976 nm excitation showed a relatively strong and broad peak at ~1140 nm (inset in Figure 5(b)). Under 488 nm excitation, the 1140 nm peak was weak or insignificant relative to the 1535 nm feature. Measurements under both excitations were made on a Si substrate with native oxide and showed no PL feature centered at 1140 nm. In addition, 976 nm excited PL spectra for Yb^{3+} codoped Er^{3+}:Y_2O_3 thin films on high purity quartz using RE-ALD did not show a broad feature at 1140 nm. These measurements suggest that some form of Er^{3+} energy transfer to the Si substrate was responsible for the 1140 nm feature. The peak at 1140 nm could originate from energy transition from the Er^{3+} $^2H_{11/2}\rightarrow{}^4I_{11/2}$ and $^4F_{9/2}\rightarrow{}^4I_{13/2}$ levels corresponding to 1110 nm and 1150 nm, respectively. Based on the reported Er^{3+} $^4I_{11/2}$ of 3.9 ms and $^4I_{13/2}$ lifetimes of 8 ms in Er^{3+} Y_2O_3 (Ref. 25) and the fact that the Er^{3+} $^4I_{11/2}$ energy level was directly pumped by the 976 nm source, an energy transition from the Er^{3+} $^4F_{9/2}\rightarrow{}^4I_{13/2}$ levels was more likely. As the radiative emission rate for the Er^{3+} $^4F_{9/2}\rightarrow{}^4I_{13/2}$ transition was weak based on spectra under 488 nm excitation, the ~1140 nm feature was attributed to efficient energy transfer from Er^{3+} $^4F_{9/2}\rightarrow{}^4I_{13/2}$ to the Si substrate.

Nanostructuring studies were performed using four different Y_2O_3:Er_2O_3 deposition sequences: *b*:*b*, 10:*c*, 15:*d*, and *f*:5. Figure 6 shows the normalized PL as a function of Er concentration and effective PL yield as a function of Er_2O_3 thickness under 488 nm excitation. At Y_2O_3:Er_2O_3 = 10:*c* and 15:*d*, an increase in the Er_2O_3 cycles, *c* or *d*, resulted in increases in the Er concentration and Er_2O_3 thickness. Quenching resulted in normalized PL reductions by a factor of 14 with increasing Er concentration and was attributed to strong $Er^{3+}\leftrightarrow Er^{3+}$ energy migration in the local Er_2O_3 layers. Interestingly, at Y_2O_3:Er_2O_3 = *b*:*b*, the normalized PL exhibited a decrease by a factor of 2 then a significant increase by 19 fold as the Er concentration increased. For this deposition sequence, the highest Er concentration of 11.8 at. % was determined to have a local Er_2O_3 thickness of 0.7 Å. This suggested that under 488 nm excitation, strong luminescence quenching was attributed to local $Er^{3+}\leftrightarrow Er^{3+}$

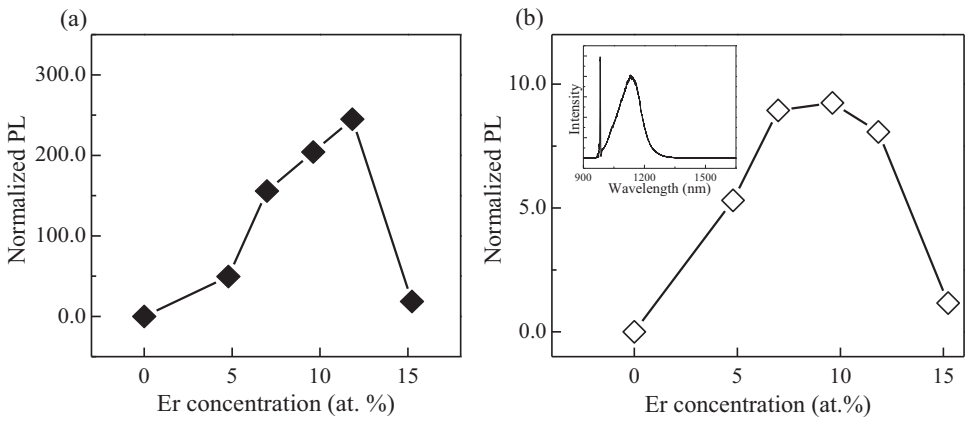

FIG. 5. Normalized PL of Er^{3+}:Y_2O_3 films synthesized with an Y_2O_3:Er_2O_3 = *a*:1 cycle sequence under (a) 488 nm excitation at 800 mW and (b) 976 nm excitation at 1500 mA.

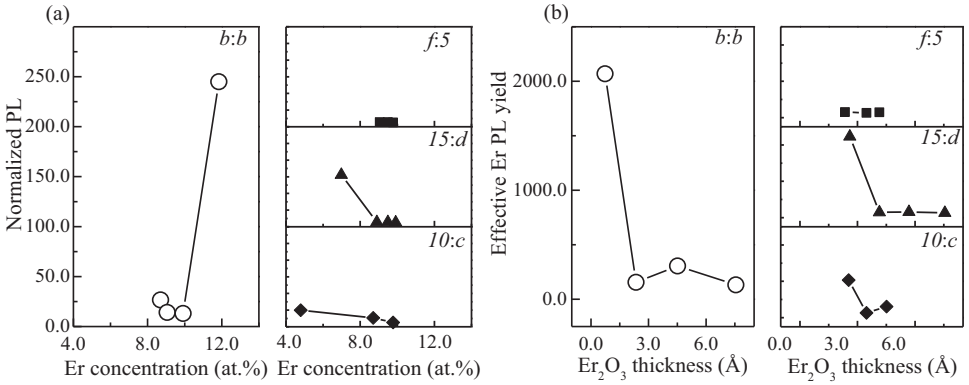

FIG. 6. Integrated PL with 488 nm excitation at 800 mW for the nanostructuring studies of Er^{3+}:Y_2O_3 films synthesized with various Y_2O_3:Er_2O_3 cycle sequence: *b*:*b*, 10:*c*, 15:*d*, and *f*:5. (a) The normalized PL yield as a function of Er concentration and (b) the effective Er PL yield as a function of Er_2O_3 thickness [ticks for sub-plots share same value as main plot].

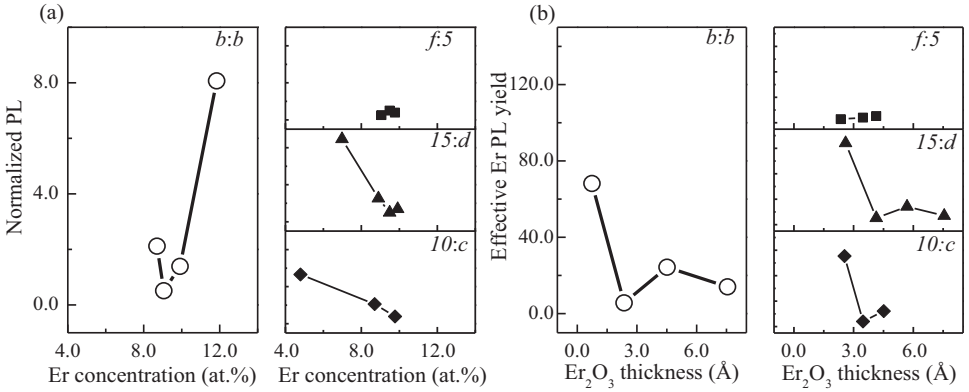

FIG. 7. Integrated PL under 976 nm excitation at 1500 mA for the nanostructuring studies of Er^{3+}:Y_2O_3 films synthesized with various Y_2O_3:Er_2O_3 cycle sequence: *b*:*b*, 10:*c*, 15:*d*, and *f*:5. (a) The normalized PL yield as a function of Er concentration and (b) the effective Er PL yield as a function of Er_2O_3 thickness [ticks for sub-plots share same value as main plot].

intralayer energy migration rather than Er_2O_3 interlayer energy migration.

For all deposition sequences studied, it was found that the Er PL yield was reduced when Er_2O_3 nanostructuring was introduced. Specifically, the effective PL yield at Y_2O_3:Er_2O_3 = *b*:*b*, 10:*c*, and 15:*c* was reduced by a factor of 17 when the Er_2O_3 thickness increased from 0.7 to 7.5 Å. At Y_2O_3:Er_2O_3 = *f*:5, quenching was observed for all films studied. These results indicated that strong $Er^{3+} \leftrightarrow Er^{3+}$ excitation migration within local nanostructured Er_2O_3 layers could lead to luminescence quenching. This strong migration was evident when the number of consecutive Er_2O_3 deposition cycles was 5 or more. Based on the Er_2O_3 thicknesses studied, strong quenching was observed for Er_2O_3 thicknesses greater than 2.4 Å.

Under 976 nm excitation, studies of Er_2O_3 nanostructuring showed that the effective Er PL yield followed a similar trend to the 488 nm excitation case as shown in Figure 7. The effective Er PL yield was reduced by a factor of 20 when the Er_2O_3 thicknesses changed from 2.5 to 7.6 Å. Again, the normalized PL as a function of Er concentration showed similar trends to the 488 nm measurements for all Er^{3+}:Y_2O_3 films. Introduction of a local Er_2O_3 layer with a thickness greater than 2.4 Å resulted in reduction in the normalized PL by a factor of 17. For Er^{3+}:Y_2O_3 deposited with the *b*:*b* cycle sequence, an increase in the normalized PL by a factor of $\sim 8\times$ was achieved when the Er concentration increased to 11.8 at. %. The lower increase in enhancement compared to that observed under 488 nm excitation was attributed to a relatively smaller Er^{3+} $^4I_{11/2}$ cross section and luminescence quenching through energy transfer from Er^{3+} to the Si substrate.

IV. CONCLUSION

In summary, Er^{3+} doped Y_2O_3 thin films with controlled nanostructuring, spatial distribution, and Er concentration were deposited in a sequential fashion using RE-ALD. The normalized PL peaked at 11.8 at. % Er under 488 nm excitation and at 9.6 at. % Er under 976 nm excitation. These concentrations were higher than previously reported and were attributed to controlled Er_2O_3 nanostructuring. By keeping the average thickness of the Er_2O_3 layers below the minimum $Er^{3+} \leftrightarrow Er^{3+}$ interaction distance of 3.5 Å, strong excitation migrations were localized to Er^{3+} ions in each Er_2O_3 layer. Interlayer $Er^{3+} \leftrightarrow Er^{3+}$ energy transfer can be reduced by increasing the spacing between the Er_2O_3 layers through the deposition of thicker layers of Y_2O_3. It was found that the PL yield increased as the Er_2O_3 layers were separated by larger Y_2O_3 thicknesses. For Er_2O_3 thicknesses greater than 2.4 Å, nanostructuring resulted in luminescence quenching by factors of 17 and 13 under 488 nm and 976 nm excitations, respectively. In addition under 976 nm excitation, it was speculated that additional PL quenching originated from Er^{3+} to Si migration evident from a strong PL feature centered at 1140 nm. The results showed that control of the nanostructuring, oxide layer spacing, and RE concentrations can be used to tailor the optical properties of thin films. These findings have important implications in the design of complex nanostructured heterogeneous optical material.

ACKNOWLEDGMENTS

The authors acknowledge the financial support from National Science Foundation under NSF CBET-0522534.

This work was carried out in part at the Stanford Synchrotron Radiation Laboratory, a national user facility operated by Stanford University on behalf of the U.S. Department of Energy, Office of Basic Energy Sciences. J. Hoang acknowledges the Dissertation Year Fellowship support from UCLA Graduate Division. He also acknowledges Calvin Pham and Ryan Hoekstra for their contributions with the experiments and PL measurements, respectively.

[1]C. Strumpel, M. McCann, G. Beaucarne, V. Arkhipov, A. Slaoui, V. Svrcek, C. del Canizo, and I. Tobias, Sol. Energy Mater. Sol. Cells **91**(4), 238–249 (2007).
[2]A. Polman, J. Appl. Phys. **82**(1), 1–39 (1997).
[3]E. F. Schubert and J. K. Kim, Science **308**(5726), 1274–1278 (2005).
[4]P. Urquhart, J. Optoelectron. **135**(6), 385–402 (1988).
[5]Y. H. Wang and J. Ohwaki, Appl. Phys. Lett. **63**(24), 3268–3270 (1993).
[6]G. N. van den Hoven, R. Koper, A. Polman, C. van Dam, J. W. M. van Uffelen, and M. K. Smit, Appl. Phys. Lett. **68**(14), 1886–1888 (1996).
[7]R. T. Wegh, E. V. D. van Loef, and A. Meijerink, J. Lumin. **90**(3–4), 111–122 (2000).
[8]A. Polman, in *28th European Conference on Optical Communication, ECOC 2002* (IEEE Cat. No. 02TH8640, Vol. 4–5 (1900)) (2002), 1 pp.
[9]D. L. Dexter and J. H. Schulman, J. Chem. Phys. **22**(6), 1063–1070 (1954).
[10]E. Snoeks, P. G. Kik, and A. Polman, Opt. Mater. **5**(3), 159–167 (1996).
[11]L. Winkless, R. H. C. Tan, Y. Zheng, M. Motevalli, P. B. Wyatt, and W. P. Gillin, Appl. Phys. Lett. **89**(11), 111115 (2006).
[12]B. Jaskorzynska, S. Sergeyev, M. Swillo, and D. Khoptyar, Acta Phys. Pol. A **99**(1), 147–153 (2001).
[13]P. G. Kik and A. Polman, J. Appl. Phys. **93**(9), 5008–5012 (2003).
[14]R. S. Quimby, W. J. Miniscalco, and B. Thompson, Fiber Laser Sources Amplifiers III **1581**, 72–79 (1992).
[15]G. N. van den Hoven, E. Snoeks, A. Polman, C. van Dam, J. W. M. van Uffelen, and M. K. Smit, J. Appl. Phys. **79**(3), 1258–1266 (1996).
[16]T. T. Van and J. P. Chang, Appl. Phys. Lett. **87**(1), 011907 (2005).
[17]T. T. Van, J. Hoang, R. Ostroumov, K. L. Wang, J. R. Bargar, J. Lu, H. O. Blom, and J. P. Chang, J. Appl. Phys. **100**(7), 073512 (2006).
[18]R. Serna, M. J. de Castro, J. A. Chaos, C. N. Afonso, and I. Vickridge, Appl. Phys. Lett. **75**(26), 4073–4075 (1999).
[19]T. Forster, Radiation Research Supplement. **2**, 326–339 (1960).
[20]D. L. Dexter, J. Chem. Phys. **21**(5), 836–850 (1953).
[21]G. N. Van den hoven, E. Snoeks, A. Polman, J. W. M. Vanuffelen, Y. S. Oei, and M. K. Smit, Appl. Phys. Lett. **62**(24), 3065–3067 (1993).
[22]T. T. Van and J. P. Chang, Appl. Surf. Sci. **246**(1–3), 250–261 (2005).
[23]J. W. Elam, Z. A. Sechrist, and S. M. George, Thin Solid Films **414**, 43–55 (2002).
[24]S. Cueff, C. Labbe, J. Cardin, J.-L. Doualan, L. Khomenkova, K. Hijazi, O. Jambois, B. Garrido, and R. Rizk, J. Appl. Phys. **108**, 0604302 (2010).
[25]M. J. Weber, Phys. Rev. **171**(2), 283 (1968).